



Fatigue crack growth in additive manufactured products

A. Riemer, H. A. Richard, J.-P. Brüggemann, J.-N. Wesendahl

University of Paderborn, Institute of Applied Mechanics

In close collaboration with Direct Manufacturing Research Center (DMRC)

riemer@fam.upb.de

ABSTRACT. Additive Manufacturing (AM) is a new innovative technique that allows the direct fabrication of complex, individual, delicate and high-strength products, based on their 3D data. Selective Laser Melting (SLM) is one of the AM processes that generates metallic components layer by layer using powder-bed technique. The irradiation and consequent melting of metallic powder is realised by the laser source. Employing SLM, especially complex and individual products, such as implants or aerospace parts, are well suited for economic production in small batches.

The first important issue in this work was to analyse the fatigue crack growth (FCG) in titanium alloy Ti-6-4 and stainless steel 316L processed by SLM. As a first step, stress intensity range decreasing tests were performed on SLM samples in their “as-built” condition. The next step was to adopt measures for optimisation of fatigue crack growth performance of SLM parts. For this purpose various heat treatments such as stress relief annealing and hot isostatic pressing (HIP) were applied to the CT specimens. Finally, the strong impact of heat treatment on the residual lifetime was demonstrated by numerical fatigue crack growth simulations. For this purpose, the hip joint implant consisting of Ti-6-4 and processed by SLM was taken into account.

It was found that residual stresses have a strong influence on the crack growth in Ti-6-4, while the influence of the micro-pores on the threshold values remains low. In contrast the results for 316L show that its fracture-mechanical behaviour is not affected by residual stresses, whereas the microstructural features lead to modification in the $da/dN-\Delta K$ -data.

The second fundamental aim of this work was to demonstrate the possibilities of the SLM process. For that reason, the individually tailored bicycle crank was optimised regarding its weight and local stresses and finally manufactured using the SLM system. The iterative optimisation procedure was based on static and cyclic loading situations as well as displacements obtained by results from numerical analyses.

KEYWORDS. Selective Laser Melting; Fatigue crack growth; Threshold value; Lightweight structure; Residual lifetime.

INTRODUCTION

The first machines for Additive Manufacturing (AM) have already been introduced in the 80s. Low build-up rates and resolutions as well as inadequate surface quality and material properties were the reason for optimising the whole process chain [1,2]. Since then, the machines have been developed continuously [1,3]. For a long time this process has been mainly used for manufacturing of prototypes. The ongoing improvement and the promising outlook for the future [4] made the AM processes attractive for universities and manufacturing companies.

For all AM-processes is common that part production is based on the CAD model which has to be designed or obtained using 3D-scans in the step before manufacturing. The AM process is characterized by material efficiency and a short time for marketing of AM components. The reasons for these advantages may be found in the following points:

- Material efficiency is realized by part manufacturing only in solid areas corresponding to the CAD model. In some AM processes like SLM the excess and unfused powder material may be sieved following part manufacturing and reused in subsequent process operations. Thus, the amount of waste material is reduced to a minimum.
- Using the direct manufacturing of parts from a CAD model, there is no need for the development and manufacturing of tools and casting molds. Consequently, the time for marketing is decreased.

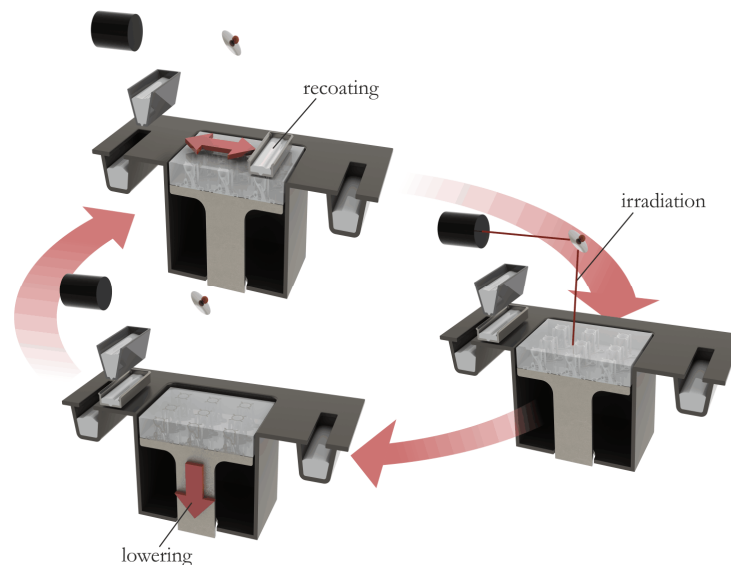


Figure 1: Basic steps of SLM-process.

The additive manufacturing process Selective Laser Melting is characterized by transition of powdered material into solid part following being irradiated by the laser source. The melt pool within this process is extended only in a small local area. Hence, layer-by-layer manufacturing of complex and delicate components becomes possible. The fabrication of parts by SLM is an iterative process that is divided into three consecutive steps, Fig. 1, as follows:

- **Recoating**: This step in the process involves the deposition of powder; either directly on the building platform within the first recoating step or on the previously deposited and irradiated powdered material in each subsequent step.
- **Irradiation**: Here, the powdered material becomes locally melted by the laser energy and bonded with the subjacent – already solidified – material. The irradiated regions here correspond to the volume areas of the CAD model. The SLM process includes various exposure strategies which have strong impact on the evolution of the material condition (i.e. residual stresses and porosity) [5,6].
- **Lowering**: This step characterizes the lowering process of the building platform and thus of the entire powder bed. The lowering value here corresponds to the thickness value of one layer selected for the fabrication. The space resulting from the lowering of the platform and the powder bed may be used in the next step for powder deposition.

Despite numerous advantages and unique features of the SLM process, the success and implementation of this technology depends mainly on its behaviour under loading. Thus, there is a real need to examine SLM materials and to optimise them. For that reason crack growth analyses on titanium alloy Ti-6-4 and stainless steel 316L were carried out.

SAMPLE MANUFACTURING

For the production of Ti-6-4 and 316L samples the Selective Laser Melting machine SLM250^{HL} (SLM Solutions) was used. The mounted laser is an ytterbium fiber laser with a maximum power of 400 watts. The data file preparation for the selective melting machine was realized by the commercial software SLM AutoFab (Marcam



Engineering). The layer thickness within the manufacturing process was 30 μm . In order to avoid contamination of powder with oxygen and nitrogen, the build chamber was filled with argon. The particle size, particle shape and particle size distribution are illustrated in Fig. 2. Here the average particle size is about 40 μm .

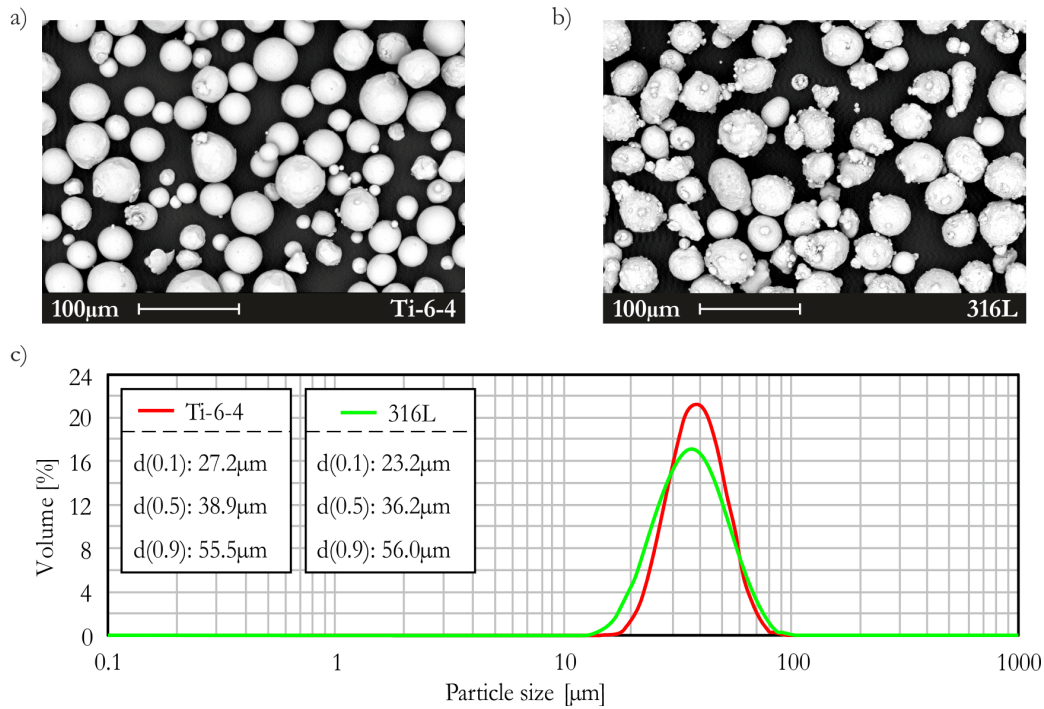


Figure 2: Metallic powder for SLM process. Scanning electron microscope images of titanium alloy powder particles a) and stainless steel powder particles b). The average particle sizes as well as the particle size distribution are depicted in c).

Employing metallic powder shown in Fig. 2 specimens with perpendicular ($\text{CD} \perp \text{BD}$), Fig. 3a, as well as parallel ($\text{CD} \parallel \text{BD}$), Fig. 3b, crack orientation with respect to the build direction were manufactured in order to draw conclusions about the level of anisotropy. Fig. 3c shows raw parts used for manufacturing the CT specimens by contour machining in both considered variants of orientation.

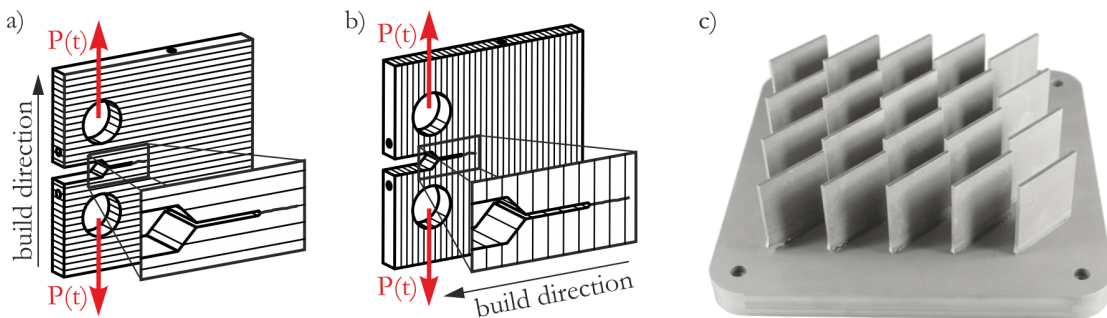


Figure 3: Orientation of build and initial crack direction. Depending on the machining of samples from the plates shown in c) specimens with crack plane normal a) and parallel b) to the build direction were processed.

CHARACTERISATION AND OPTIMISATION OF FRACTURE-MECHANICAL PERFORMANCE

The major intention of present work is to show that employing SLM for part production material properties in range of conventionally processed materials are available. In order to meet this goal, studies on compact tension specimens processed of titanium alloy Ti-6-4 and stainless steel 316L were performed. Furthermore, the effect of

pores and residual stresses on the crack growth performance has been analysed. Therefore the CT specimens were subjected to different heat treatments aimed at stress relieving and pore reduction respectively.

Titanium alloy Ti-6-4

The fracture-mechanical performance of parts produced by SLM depends on the material used. For Ti-6-4 in its untreated condition low and insufficient crack growth data was found. For this material heat treatment is necessary. Fig. 4a and b show the results for threshold values for various heat treatments in both examined orientations. The threshold values are plotted vs. Yield strength and Elongation at break respectively (for more details cf. [7]). Fig. 4c illustrates the crack path in as-built (that means untreated condition) and 800° (that means following heat treatment at 800°C) condition. For as-built condition high residual stress in range of the Yield strength were found by X-Ray diffraction measurements. These high residual stresses have huge influence on the threshold values, Fig. 4a and b, as well as on the crack path, Fig. 4c. For the material condition resulting from the heat treatment at 800°C hardly any residual stresses were found. This is the reason for crack growth direction in line with notch direction following treatment at 800°C. Additionally, Fig. 4a and b include the results for the treatment at the higher temperature of 1050°C where modifications in microstructure were achieved. In this case, the highest level of anisotropy (despite heat treatment) was found. Within the HIP treatment (hot isostatic pressing) the samples were applied to high temperature and pressure. This ensures that residual stresses are removed and micro-pores partly compressed.

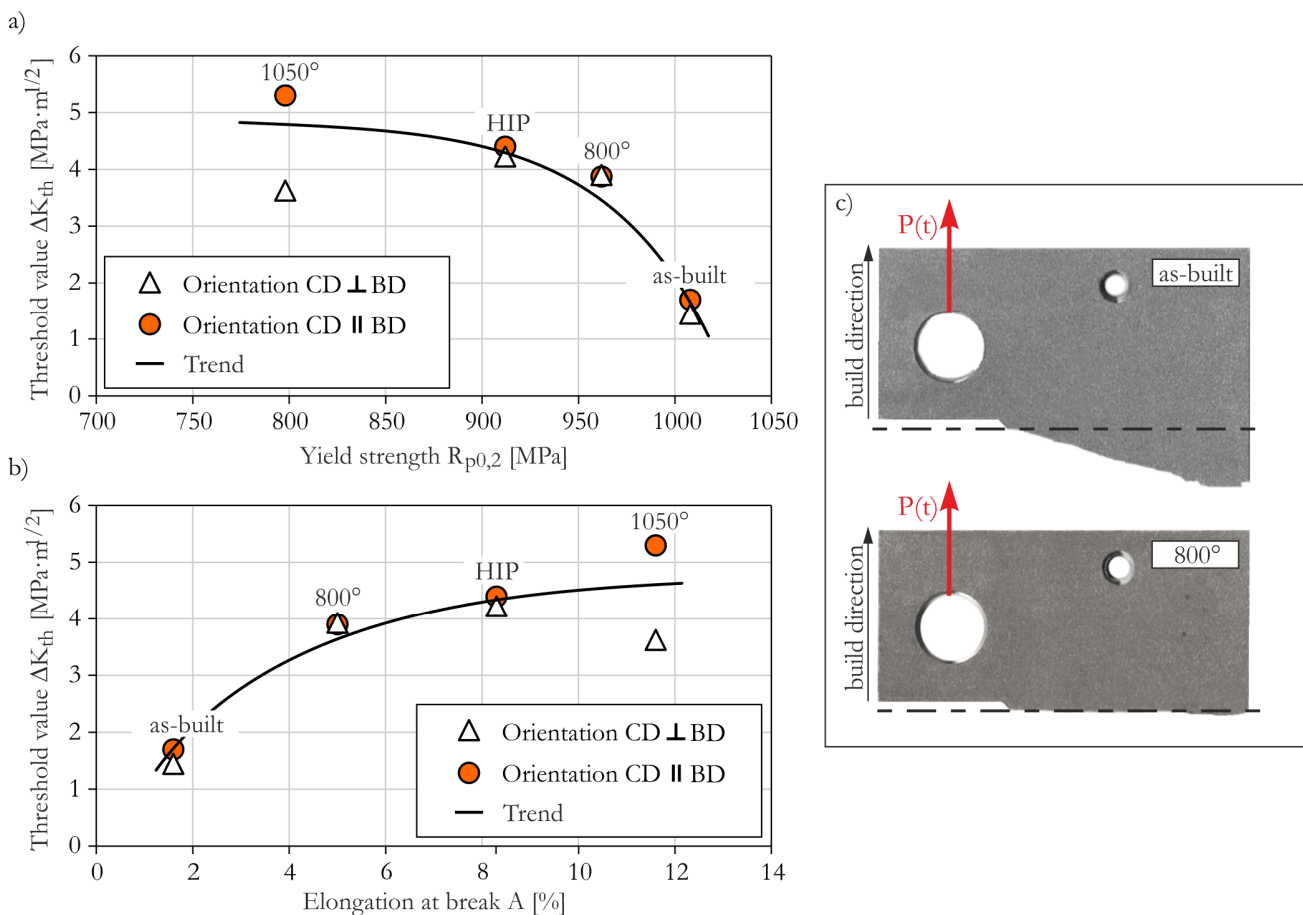


Figure 4: The dependence of threshold values on the Yield strength a) and Elongation at break b). The effect of the residual stresses on the crack path is shown in c).

In order to classify the fracture-mechanical data obtained for selective laser melted Ti-6-4 tests for conventionally processed material were carried out. In these tests a threshold value of 3.3 MPa·m^{1/2} was found. Furthermore, in literature a value of 4.0 MPa·m^{1/2} for Ti-6-4 processed by conventional techniques is published. The findings from tests on laser melted Ti-6-4 show that residual stresses have the major influence on the fracture-mechanical performance of Ti-6-4. Heat treatment is absolutely necessary in order to reduce residual stresses and consequently to achieve or even to exceed

the threshold values for conventionally processed material. The fatigue crack growth curves and further details for the static and fatigue data as well as for the influence of Hot Isostatic Pressing (HIP) on porosity and residual stresses are presented in [7].

Stainless steel 316L

For the material 316L the level of anisotropy in the as-built condition is higher than for titanium alloy. The threshold values vary from $3.0 \text{ MPa}\cdot\text{m}^{1/2}$ for CD \parallel BD to $4.3 \text{ MPa}\cdot\text{m}^{1/2}$ for CD \perp BD, Fig. 5a and b. Moreover, the threshold values are not affected by the heat treatment at 650°C which aims at the stress relieving, Fig. 5b. Following heat treatment at 650°C , the residual stresses were found to be reduced by half, cf. [8]. Consequently, the internal stresses do not seem to affect the crack growth performance of stainless steel. The threshold values of 316L could only be improved by application of Hot Isostatic Pressing. Moreover, the anisotropy in threshold values was eliminated completely by the use of HIP process, Fig. 5b. Furthermore, the values were increased due to the HIP treatment compared to the threshold values for the as-built condition.

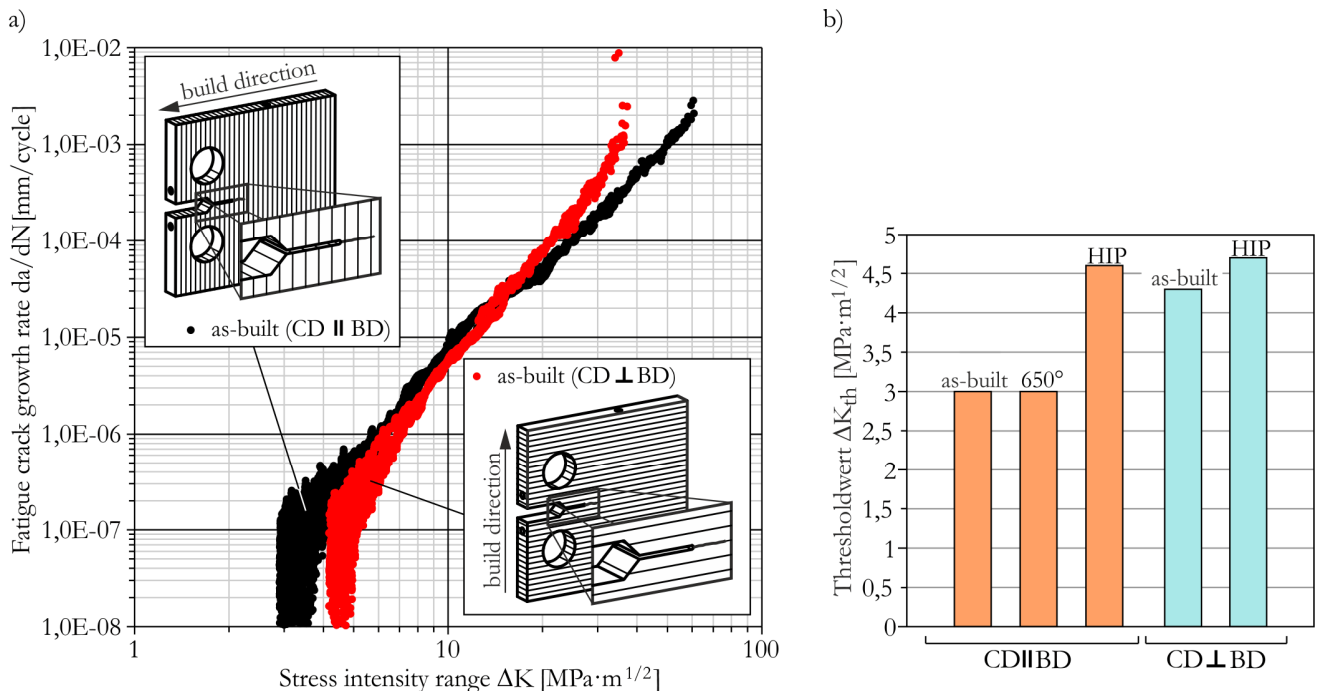


Figure 5: Crack growth curves for the as-built condition and the orientations CD \perp BD and CD \parallel BD a) and the threshold values following heat treatments b).

In further studies it was shown that in case of 316L the process-specific microstructure shows the highest influence on the evaluation of fracture-mechanical data. More details concerning the effect of microstructure on the crack growth data may be deduced from [8].

NUMERICAL CRACK GROWTH ANALYSIS

In this study, the effect of treatment (and consequently of the residual stresses) was analysed. For that reason titanium alloy Ti-6-4 in the conditions as-built and 800° was examined. The required fatigue crack growth data was obtained from [7] and characterised by the FORMAN/METTU-equation. Afterwards, this mathematical description was implemented into numerical crack growth simulation program ADAPCRACK3D [9].

The object for the lifetime study is the hip joint implant. This part has to be personalised and consequently suitable for production employing the SLM process. The boundary conditions used for the crack growth simulation are presented in Fig. 6 schematically. These boundary conditions correspond to the load case “Normal Walking” and are in accordance with the mechanical models developed by Pauwels [10]. Therefore, the initial crack in the region where the highest

principal stresses occur, Fig. 6, and the R-ratio of 0.1 are assumed. Furthermore, details regarding the mesh are presented in Fig. 6.

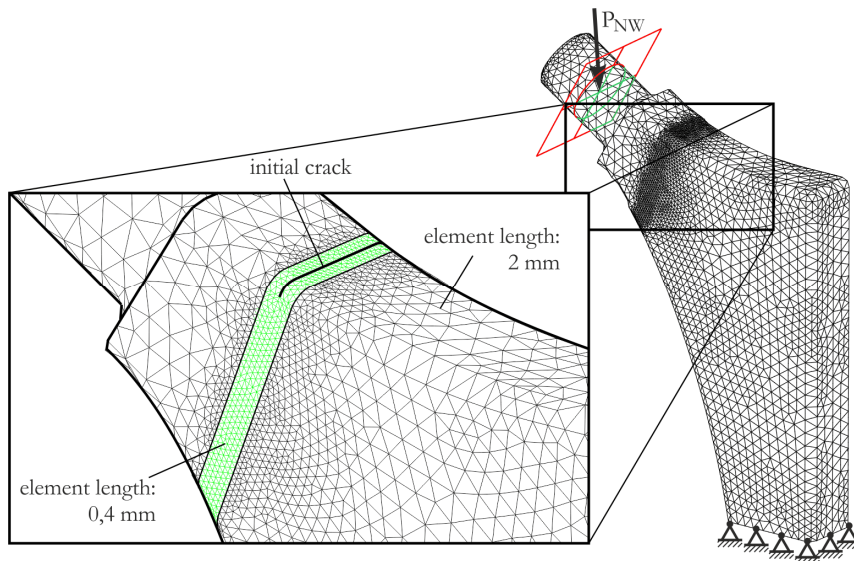


Figure 6: FE-model of the implant with its boundary conditions and meshing details.

Fig. 7 presents the crack path, the stress distribution and the crack length in the last simulation step before the unstable crack growth begins. This simulation was performed based on the body weight of 80 kg. The results of crack growth simulation show significant differences in the remaining lifetime, c.f. Fig. 7. In the as-built condition the fracture occurs at 100000 cycles. Following the heat treatment at 800°C the unstable crack growth begins at 2.5 millions of cycles. Consequently, the increase in the lifetime is possible due to a treatment at 800°C. Here, the lifetime extension was found by a factor of about 25. That means that from the fracture mechanical point of view, technical parts consisting of Ti-6-4 require heat treatment aiming at residual stress reduction.

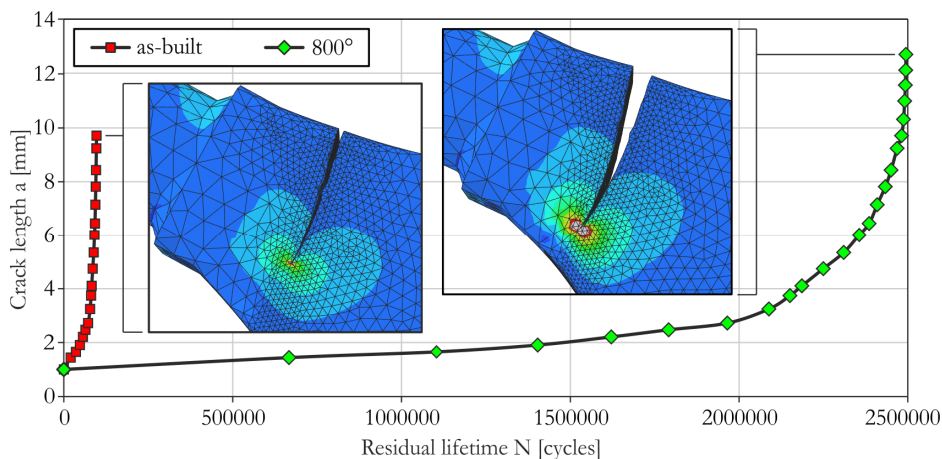


Figure 7: Numerical crack growth simulation depending on the material condition.

WEIGHT AND STRENGTH OPTIMISATION OF A BICYCLE CRANK

The bicycle crank has been selected to be optimised by numerical studies and to be manufactured by Selective Laser Melting. The optimisation regarding weight and strength is based on biomechanical studies that were carried out at the Institute of Applied Mechanics (FAM). In these studies was found that tall people need long bicycle cranks for better transmission ratios. The optimisation of the structure within this work is based on the consideration of static



loading defined in the German standard DIN EN ISO 4210-8 and on the cyclic loading that was deduced from [11]. In the last step, the final geometry was selected under consideration of the balance between low deformation and weight.

Crank and section geometry

The standard crank lengths available on the market range from 165 mm to 180 mm. The length used for analyses and fabrication in this work was 200 mm, cf. Fig. 8a. The area of modification was defined in order to vary the cross-sectional geometry. In regions outside the modification area bulk material was defined due to high local loadings that occur in these regions.

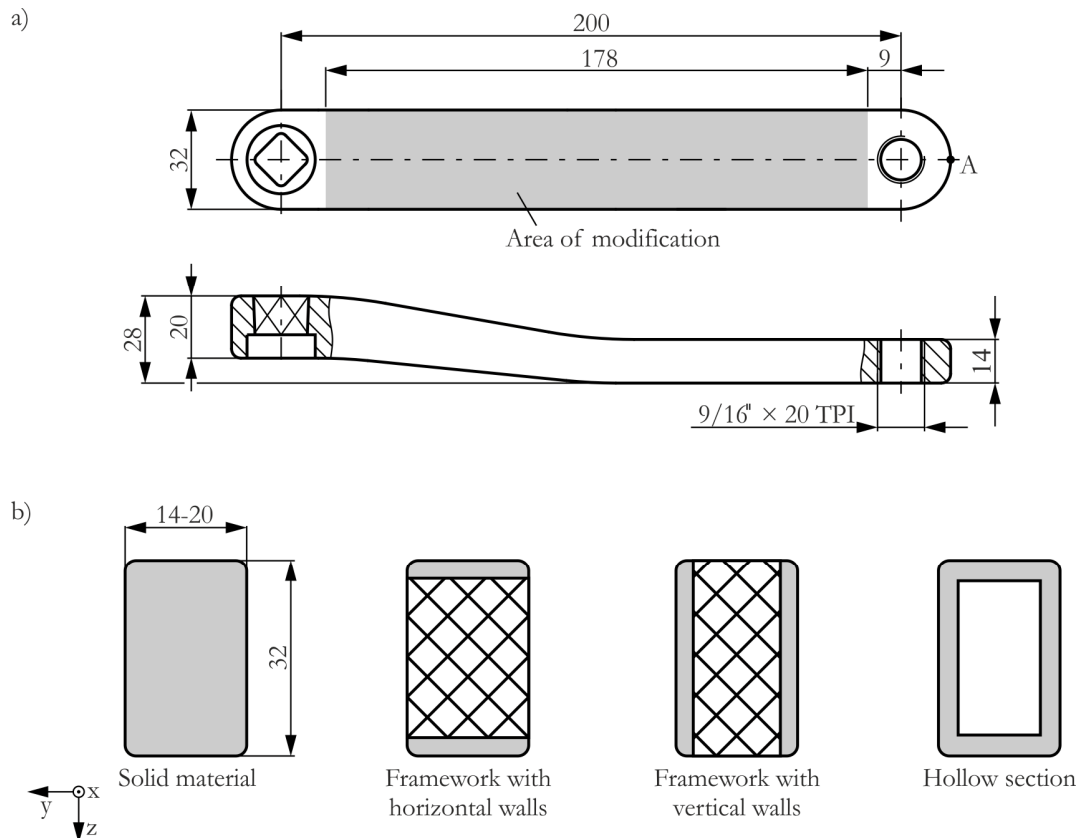


Figure 8: Dimensions of the personalised bicycle crank a) and variants of geometry for the cross section in the area of modification b).

The variants used to figure out the most suited cross section are illustrated in Fig. 8b. The cross section consisting of solid material is used as reference. In this case, the highest weight as well as lowest local stresses and displacements occur. The both variants with horizontal and vertical walls contain framework that stabilises the walls. The last variant represents a hollow cross section. This geometry is well suitable for bending and torsion.

Determination of the most suitable cross section

In a first step a loading of 1500 N was applied to the FE-Models of the various variants presented in Fig. 8. The selected boundary conditions correspond to DIN EN ISO 4210-8. The material used in this study is Ti-6-4. The results for the maximum equivalent stress are presented in Fig. 9b. In these analyses, three different crank angles were taken into account. Furthermore, the limitation (456 MPa) of the stresses that occur in the bicycle crank is drawn in the diagram in Fig. 9b. For that reason a safety factor of 2 and the Yield strength of 912 MPa (cf. [7]) was used.

The solid variant shows the lowest values of maximum stresses that occur in the structure. In addition, the stresses here are in the same range for the three considered angles, cf. Fig. 9a and b. The huge difference between the limitation and loading occurring show the large potential for optimisation. The displacements for this cross section are the lowest within the considered structures, Fig. 9c. The value of 470 g for the weight, Fig. 9d, is high compared to the non-solid designs. In case of the variant "Framework with horizontal walls", the high displacement, Fig. 9c, was not acceptable. Consequently, this cross-sectional geometry was rejected. On closer examination of the designs "Framework with vertical walls" and

“hollow section” it becomes clear that due to lower maximum stresses and lower weight, the variant “hollow section” exhibits more potential for optimisation. Consequently, this structure design will be optimised in detail in following studies.

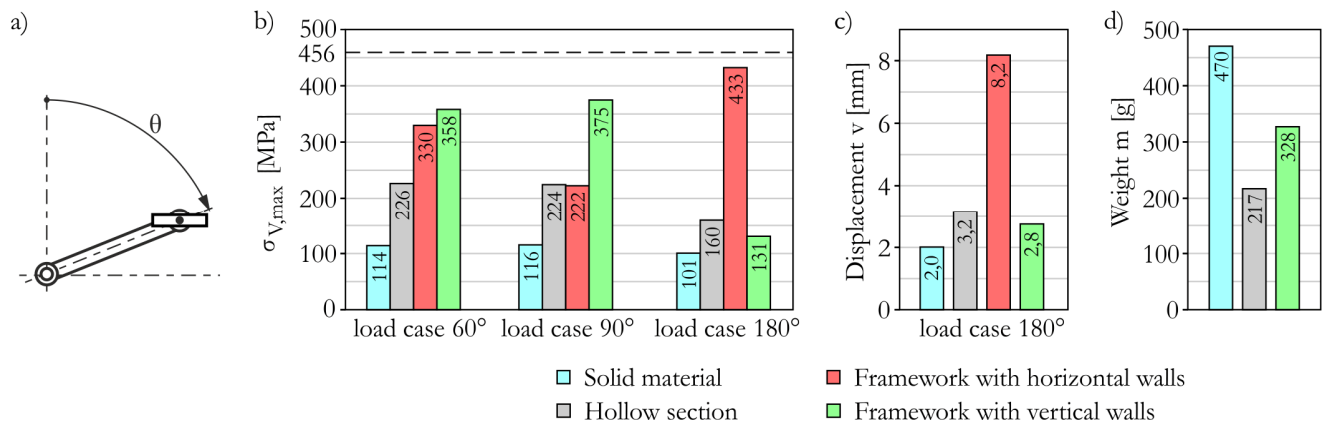


Figure 9: Numerical stress analysis results for different load cases b) resulting from various bicycle crank angles a) and maximum displacement results c). Data for the mass are presented in d).

Detailed optimisation of the bicycle crank

The detailed optimisation of the selected variant was performed considering static and fatigue strengths. The safety factors here were reduced to a value of 1.5. In addition to titanium alloy Ti-6-4, two further materials, the stainless steel 316L and the aluminium alloy EN AW-7075-T651, were taken into account. During the optimisation process, buckling problems in the region of the walls occurred. For this purpose, additional walls within the hollow structure were designed, cf. Fig. 10b-d. In this way, the stiffness of this structure design was increased. The value of the thickness of interior walls was kept constant at 1 mm. The results of the optimisation are listed in Tab. 1. The highlighted variants represent for each material the bicycle crank with lowest weight and conditions fulfilled.

Variant	Material	Static strength	Fatigue strength	Displacement v [mm]	Weight m [g]
1 mm hollow	Ti	✓	✓	-5.6	153
1 mm hollow	Al	✗	✗	-9.2	97
1 mm hollow	St	✗	✓	-3.5	278
1 mm walls		✓	✓	-4.9	187
0.8 mm walls	Ti	✓	✓	-5.6	177
0.7 mm walls		✓	✓	-6.1	171
2 mm walls		✓	✓	-1.9	453
1.7 mm walls		✓	✓	-2.1	420
1.5 mm walls	St	✗	✓	-2.3	398
1 mm walls		✗	✓	-3	340
2 mm walls		✓	✓	-5	158
1.5 mm walls	Al	✓	✓	-6	139
1 mm walls		✗	✗	-8	119
		✓ Condition fulfilled	✗ Condition not fulfilled		

Table 1: Results of part optimisation based on numerical studies.

Parts consisting of stainless steel show the largest values for weight. Consequently, they shouldn't be manufactured by Selective Laser Melting. The aluminium alloy represent excellent lightweight properties and due to the lack of processing parameters, efforts have to be made in order to realise the part production by the use of EN AW-7075-T651. The parts consisting of titanium alloy deliver small masses. Consequently, the laser melted Ti-6-4 should be employed in lightweight applications. In this study, the design with the thickness value of 0.8 mm for outer walls was selected for fabrication by SLM. This variant has well-balanced values regarding low displacement and weight.

Part manufacturing and non-destructive testing

Figure 10a show the bicycle cranks in their final design positioned on the substrate platform. These parts are connected to the platform by support structures. Supports are used to keep the SLM parts and the overhanging surfaces in position, to transfer the heat from the melt pool and to counteract the distortion that occurs due to the residual stresses.

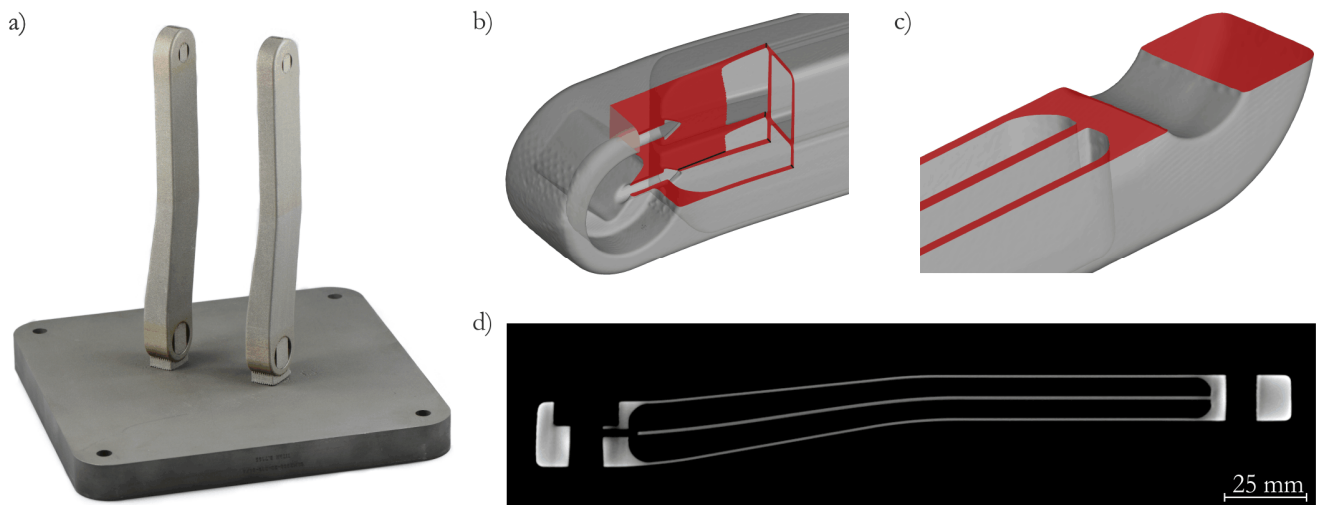


Figure 10: Final product positioned on the substrate platform a) and the nondestructive test results from the computer tomography b), c) and d).

In order to examine the bicycle crank in its interior area Computer Tomography (CT) scans were performed. The maximum resolution in this analysis was limited to 200 μm . The aim was to exclude imperfections like macro pores, cracks and distortions of internal structures. The interior chambers as well as holes that are required in order to remove the powder material out of the chambers are presented in Fig. 10b. Fig. 10c shows that no collapse of the overhanging areas occurs. The bicycle crank following fabrication corresponds to the CAD model. Fig. 10d illustrates the final design in half-section where the thin walls exhibit constant thickness.

CONCLUSIONS

The present work proves that the Selective Laser Melting technique has promising opportunities for the future. The fracture mechanical properties may be optimised by the application of subsequent treatments.

The residual stresses which occur in the titanium alloy have a very high influence on the crack growth. Parts consisting of Ti-6-4 should be heat treated (for example at 800°C) in order to achieve a significant improvement in crack growth performance and to exceed the crack growth data that was found for conventionally processed material. By means of the crack growth simulation was found that the remaining lifetime may be increased by a factor of 25.

Stainless steel shows a low level of dependency upon heat treatment that aims at stress relieving. The crack growth performance is influenced to a large extent by the microstructure. This can be deduced from the different threshold values from the both orientations used in this study and from the increased threshold values following HIP process that results in a modified microstructure.

The studies focused on the optimisation of the bicycle crank show the large lightweight potential of the SLM technique. Especially, personalised, delicate and geometrically complex parts are obvious candidates for fabrication by SLM.



REFERENCES

- [1] Levy, G.N., Schindel, R., Kruth, J.P., Rapid manufacturing and rapid tooling with layer manufacturing (LM) technologies, state of the art and future perspectives, *CIRP Annals - Manufacturing Technology*, 52 (2003) 589–609.
- [2] Ziemian, C.W., Crown, P.M., Computer aided decision support for fused deposition modeling, *Rapid Prototyping Journal*, 7 (2001) 138–147.
- [3] Kruth, J.-P., Leu, M.C., Nakagawa, T., Progress in Additive Manufacturing and Rapid Prototyping, *CIRP Annals - Manufacturing Technology*, 47 (1998) 525–540.
- [4] Gausemeier, J., Echterhoff, N., Kokoschka, M., Wall, M., Thinking ahead the Future of Additive Manufacturing – Analysis of Promising Industries, Study for the Direct Manufacturing Research Center, Paderborn, (2011).
- [5] Kruth, J.-P., Deckers, J., Yasa, E., Wauthlé, R., Assessing and comparing influencing factors of residual stresses in selective laser melting using a novel analysis method, *Journal of Engineering Manufacture*, 226 (2012) 980-991.
- [6] Matsumoto, M., Shiomi, M., Osakada, K., Abe, F., Finite element analysis of single layer forming on metallic powder bed in rapid prototyping by selective laser processing, *International Journal of Machine & Manufacture*, 42 (2002) 61-67.
- [7] Leuders, S., Thöne, M., Riemer, A., Niendorf, T., Tröster, T., Richard, H.A., Maier, H.J., On the mechanical behaviour of titanium alloy TiAl6V4 manufactured by selective laser melting: Fatigue resistance and crack growth performance, *International Journal of Fatigue*, 48 (2013) 300-307.
- [8] Riemer, A., Leuders, S., Thöne, M., Richard, H.A., Tröster, T., Niendorf, T., On the fatigue crack growth behavior in 316L stainless steel manufactured by selective laser melting, *Engineering Fracture Mechanics*, 120 (2014) 15-25.
- [9] Schöllmann, M., Fulland, M., Richard, H.A., Development of a new software for adaptive crack growth simulations in 3D structures, *Engineering Fracture Mechanics*, 70 (2003) 221-230.
- [10] Pauwels, F., *Biomechanics of the Locomotor Apparatus. Contributions on the Functional Anatomy of the Locomotor Apparatus.* Springer-Verlag, Berlin Heidelberg New York, (1980).
- [11] Hillebrecht, M., Schwirtz, A., Stapel-Feldt, B., Stockhausen, W., Bührle, M., Tritttechnik im Radsport. Der “runde Tritt” – Mythos oder Realität?, *Leistungssport*, 6 (1998) 58-62.